applied sciences

MDPI

Article

Cardiorespiratory Response to Workload Volume and Ergonomic Risk: Automotive Assembly Line Operators' Adaptations

Dania Furk [1], Luís Silva [1,*], Mariana Dias [1], Carlos Fujão [2], Phillip Probst [1], Hui Liu [3] and Hugo Gamboa [1]

[1] Laboratory for Instrumentation, Biomedical Engineering and Radiation Physics (LIBPhys-UNL), Physics Department, Faculty of Sciences and Technology of the NOVA University of Lisbon (FCT-NOVA), 2829-516 Caparica, Portugal; daniafurk@gmail.com (D.F.); mag.dias@campus.fct.unl.pt (M.D.); p.probst@campus.fct.unl.pt (P.P.); hgamboa@fct.unl.pt (H.G.)
[2] Industrial Engineering Production System (Ergonomics Team), Volkswagen Autoeuropa, Quinta do Anjo, 2954-024 Palmela, Portugal; carlos.fujao@volkswagen.pt
[3] Cognitive Systems Lab, University of Bremen, Bibliothekstraße 1, 28359 Bremen, Germany; hui.liu@uni-bremen.de
* Correspondence: lmd.silva@fct.unl.pt

Abstract: Repetitive tasks can lead to long-term cardiovascular problems due to continuous strain and inadequate recovery. The automobile operators on the assembly line are exposed to these risks when workload volume changes according to the workstation type. However, the current ergonomic assessments focus primarily on observational and, in some cases, biomechanical methods that are subjective and time-consuming, overlooking cardiorespiratory adaptations. This study aimed to analyze the cardiorespiratory response to distinct workload volumes and ergonomic risk (ER) scores for an automotive assembly line. Sixteen male operators (age = 38 ± 8 years; BMI = 25 ± 3 kg·m^2) volunteered from three workstations (H1, H2, and H3) with specific work cycle duration (1, 3, and 5 min respectively). Electrocardiogram (ECG), respiratory inductance plethysmography (RIP), and accelerometer (ACC) data were collected during their shift. The results showed significant differences from the first to the last 10 min, where H3 had its SDRRi reduced ($p = 0.014$), H1's phase synchrony and H2's coordination between thoracic and abdominal movements decreased ($p < 0.001$, $p = 0.039$). In terms of ergonomic risk, the moderate-high rank showed a reduction in SDRRi ($p = 0.037$) and moderate-risk activities had diminished phase synchrony ($p = 0.018$) and correlation ($p = 0.004$). Thus, the explored parameters could have the potential to develop personalized workplace adaptation and risk assessment systems.

Keywords: ECG; RIP; workload; ergonomic risk; occupational health

check for updates

Citation: Furk, D.; Silva, L.; Dias, M.; Fujão, C.; Probst, P.; Liu, H.; Gamboa, H. Cardiorespiratory Response to Workload Volume and Ergonomic Risk: Automotive Assembly Line Operators' Adaptations. *Appl. Sci.* **2024**, *14*, 3921. https://doi.org/10.3390/app14093921

Academic Editor: Suchao Xie

Received: 2 April 2024
Revised: 28 April 2024
Accepted: 30 April 2024
Published: 4 May 2024

Copyright: © 2024 by the authors. Licensee MDPI, Basel, Switzerland. This article is an open access article distributed under the terms and conditions of the Creative Commons Attribution (CC BY) license (https://creativecommons.org/licenses/by/4.0/).

1. Introduction

According to a recently published report, the largest proportion of workers within the EU are employed in the manufacturing sector. On average, employees such as machine operators and assemblers work for 39.7 h per week [1]. During this time, they are engaged in physically demanding tasks that require manual material handling, exposing workers to awkward and upright postures during long periods of repetitive movement [2]. These pose risks to workers' health, particularly cardiovascular and musculoskeletal strain. Traditional ergonomic guidelines have primarily focused on biomechanical factors by assessing ergonomic risk (ER) stratification. This method is currently dominated by observational methods [3], which typically involve a specialist who watches the workers as they carry out their tasks. During observation, the specialist completes a specific worksheet that considers various body parts, task intensity, duration, and cycle frequency [4]. While these guidelines have been effective in reducing the muscular and cardiovascular load

to some extent [5], subjective measures often overlook the complexity of individual internal responses that workers experience during task execution [6], namely, their impact on cardiovascular health.

Despite the common assumption that such physical activity benefits health, emerging evidence suggests a paradoxical relationship between occupational physical activity and cardiovascular health. It has been linked with elevated blood pressure [7], atherosclerosis [8], and coronary heart disease [9], culminating in cardiovascular disease. This phenomenon is referred to as the physical activity paradox [10]. This discrepancy raises important questions about how the nature, intensity, and perception of physical activity at work impact health.

The concept of relative heart rate (RHR) has emerged as a valuable indicator of the intensity of physical work. By comparing the difference between work and rest heart rates with the reserve heart rate (maximum heart rate—rest heart rate), RHR comprehensively assesses the physiological demands placed on workers during their shifts [11]. The balance between a worker's physical capacity and their job demands can be quantified by maximum acceptable work time (MAWT). It further refines our understanding of workload by considering individual factors such as age, VO_{2max}, and work-related VO_2 [12] , helping prevent overwork-related health issues. The overwork index derived from the ratio of each operator's working time to MAWT has provided means to evaluate the risk of cerebrocardiovascular disease associated with prolonged working. Furthermore, it highlights the need to balance worker's physical abilities and task demands [13].

The measurement of these parameters in real-time has come into focus. This is made possible with the appearance of wearable technology and the integrated setting that Industry 4.0 offers. With this, the necessary means to provide proactive prevention and continuous information on the physical state has been made available to the workers and managers [14].

Past studies on assembly lines have harnessed the capabilities of this technology to ascertain job exposure to optimize productivity. In [15] and [16], the reserve heart rate was monitored through telemetry ECG. In the former, the adoption of a new work strategy decreased HR significantly [15]. In the latter, it was found that cardiovascular load was substantial for the car disassembly tasks that were being performed [16], even after including changes to the assembly line organization . Furthermore, they give a one-sided perspective of the physiological response of its workers by only measuring the reserve heart rate.

Respiratory monitoring is another physiological signal that carries insightful information. Previously, it was used to quantify relevant factors in the occupational context, such as mental load and environmental stress [17]. Louvhevaara et al. compared the effects of fatiguing dynamic and isometric hand-grip exercises on cardiorespiratory adaptations. They measured HR, blood pressure, and ventilatory gas exchange, finding relevant differences between those two types of exercise only in breathing patterns [18]. In our previous work, we aimed to evaluate respiratory and cardiovascular responses to fatigue-inducing work. To accomplish this goal, a protocol simulating repetitive work was applied in a laboratory setting. In the first study, respiratory inductance plethysmography (RIP) signals were used to explore synchrony metrics between the abdominal (ABD) and rib cage (RC) walls [19]. A second study explored the changes in heart rate variability (HRV) with increased fatigue [20]. In these, the main findings were that throughout the fatigue trials, both the synchrony between the respiratory walls and HRV were significantly reduced.

In summary, the prevalent risk quantification tools lack consideration for the cardiorespiratory response, when assembly line tasks are linked to long-term cardiovascular deterioration. The assessment of risk is performed by the workstation measuring its biomechanical load, rather than the individual response to the workload volume. The use of wearable technology has brought the capacity for individual continuous monitoring of workers' adaptations during their shifts. While the previous research has addressed some of the downsides of subjective assessments, they do not fully address the cardiorespiratory

influences as they have their main concern on productivity, falling short in exploring other variables other than reserve heart rate; are mostly conducted in laboratory settings; do not include all conditions of realistic settings; and lack actual workers in the industry. This research has the objective of bridging this gap by verifying if there are distinct cardiorespiratory responses to particular workload volumes and ERs of assembly line workers during a period of their shift. Like this, there is the possibility of more personalized work interventions, task management, and health problem prevention. In this paper, operator's adaptations refer to assembly line worker's cardiorespiratory adaptations due to their repetitive tasks. Workload volume is defined by the time in which a complete cycle of work is performed.

In the remainder of this document, the Materials and adopted Methods will be detailed in Section 2, followed by the showcase of the results in Section 3, their discussion in Section 4, and finally, the summary of the main findings and contribution.

2. Materials and Methods

This section begins with the protocol used to collect data, a general description of the activities performed during acquisitions and its participants. Following this, the methods used to process the signals and the extracted parameters are described. Finally, the statistical approach to analyze these data is explained.

2.1. Monitored Workstations

The studied factory relies on several stages of vehicle manufacturing. For this particular research, the assembly and alignment tasks were monitored, as they rely on manual processes that can bring health consequences to workers. At each workstation, specific activities are performed:

- H1—tailgate and taillight alignments and attachment of the taillights;
- H2—alignment of the side doors, rear end, and front end;
- H3—mounting of the rear-view mirror, cowltop, boot panel, and the trunk symbol.

Figure 1 shows a sequence of movements performed for each task and the specified workstation.

2.2. Participants

Sixteen workers from a car manufacturing company were selected through a voluntary participation campaign (age: 38 ± 8 yrs; body mass index: 25 ± 3 kg/m^2; physical activity: 220 ± 135 min per week), all male and right handed. The workers were recruited from three different workstations and were all part of the product assembly: H1 (4), H2 (4), and H3 (8); the procedures and objectives were explained to all participants and they read and signed informed consents.

2.3. Ergonomic Risk

Each of the tasks performed at the factory have an ergonomic risk score, something determined by the ergonomist. The European Assembly Worksheet (EAW) is the scoring worksheet used by the studied company. It includes whole-body and upper-limb assessment of risk factors, resulting in a traffic-light-like risk score estimation [21], and its scheme is represented in Figure 2.

To be able to analyze the cardiorespiratory response association with the ergonomic score, tasks were considered to be low-risk with a score equal or under 25 (green), moderate-risk with a score between 25 and 48 (yellow), and moderate–high-risk with a score equal or above 48 (orange).



Figure 1. Performed tasks at each workstation.

	SCORE	COLOR SCHEME	ACTIONS
EAWS Risk Score	0—25	Green	**Low risk:** recommended; no action needed
	>25—50	Yellow	**Possible Risk:** not recommended; redesign if possible
	>50	Red	**High Risk:** to be avoided; action to lower the risk if necessary

Figure 2. European Assembly Worksheet overall estimation scheme, adapted from [22].

2.4. Protocol

First, the volunteers were asked to read and sign the informed consent to be part of the study. Next, age, height, physical exercise habits (number of days per week, duration and type), and dominant limb were asked from each subject, and their weight was measured with a digital scale. The study was conducted in accordance with the Declaration of Helsinki, and the protocol was approved by the Ethics Committee of the University of Porto.

2.4.1. Sensor Placement

To monitor ECG, RIP, and ACC data during the operators' activities, multiple sensors had to be placed on the subject's body. Before placing the sensors, the corresponding skin areas were cleaned by hair removal, abrasion, and alcohol wiping.

The ECG sensor (PLUX WIRELESS BIOSIGNALS S.A.) was placed with three disposable adhesive Ag/AgCl electrodes (Ambu®) attached to each of its electrode cables. The positive was placed on the left side of the sternum at the level of the manubrium, the negative on the superior part of the sternum's body, and the ground electrode was placed on the left anterior superior iliac spine. The RIP sensors (PLUX WIRELESS BIOSIGNALS S.A.) were attached to two elastic belts, one placed under the chest passing the underarms and the other band at the umbillicus level [19,23], subsequently being adjusted to the participant's anatomy. On the center of the subject's lower back, a triaxial ACC (PLUX WIRELESS BIOSIGNALS S.A.) was secured with an elastic belt. The four mentioned sensors were set to acquire data at a rate of 350 Hz and were connected to the 8-channel wireless Hub (PLUX WIRELESS BIOSIGNALS S.A.).

To capture the upper limbs acceleration data, two MuscleBAN devices (PLUX WIRELESS BIOSIGNALS S.A.) were placed on the belly of the right trapezius and biceps brachii, of the worker's dominant limb, with a rate of 1000 Hz. Both the Hub and MuscleBAN devices transmitted the data acquired by each sensor to the *OpenSignals* (version Public Build 2023-10-23, PLUX WIRELESS BIOSIGNALS S.A., Lisbon, Portugal) software on a smartphone (Xiaomi Redmi Note 9, running Android 10). A scheme of the described setting is represented in Figure 3.

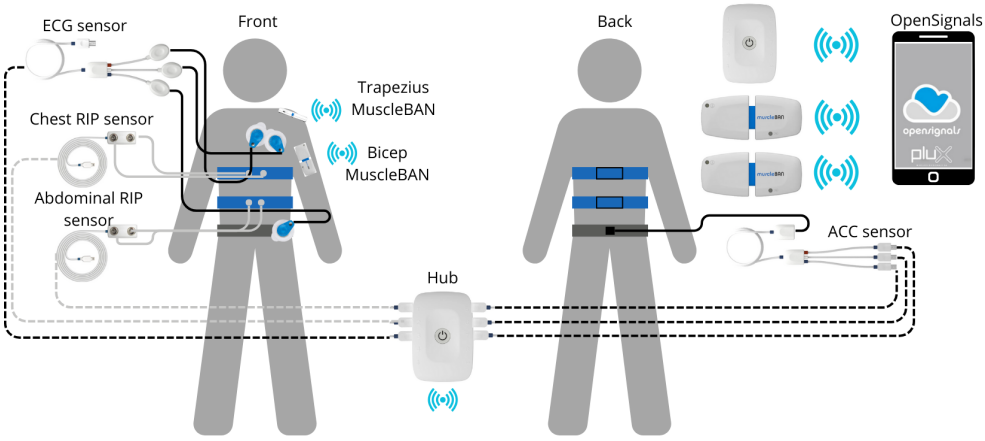


Figure 3. Sensor configuration for signal acquisition. ECG—electrocardiography; RIP—respiratory inductance plethysmography; ACC—accelerometer.

2.4.2. Signal Acquisition

Before starting the acquisition, volunteers were asked to place the mobile phone within a pocket of the uniform in such a way that it did not interfere with their work. Subsequently, the participants were asked to perform a distinctive movement (10 jumps) that was later used for data synchronization purposes. The data were collected for approximately 50 min and the first 4 to 5 cycles of the performed task were also video-taped.

2.5. Signal Processing

2.5.1. Electrocardiography

The ECG is a non-invasive way to measure the electrical activity of the heart, allowing us to extract relevant information to evaluate its state [24].

Most of the parameters computed in this study are derived from the identification of the R-peaks. Due to the ECG's characteristics changing in time and frequency, maximal overlap discrete wavelet transform (MODWT) filters have become a trend [25], being the selected method to apply to the collected signals. These filters decompose the signal into basis functions (wavelets) that contain information in both time and frequency of a signal at different resolution levels. By choosing the appropriate frequency level, we are able to remove undesired components present in the signal [25]. MODWT was preferred over traditional wavelet decomposition due to its better alignment of the reconstructed signal with the original time-series [26]. The most suitable wavelet was chosen based on the quantification of how much the R-peaks were enhanced using the maximization of the energy-to-Shannon entropy ratio criterion, proposed by He et al. [27]. Level 4 decomposition coefficients were stored and used to perform the inverse wavelet transform to reconstruct the signal and thus give us the filtered result, which corresponds to a frequency band of 11–22 Hz. The R-peak detection algorithm started with baseline shift removal and normalization of the signal amplitude. Next, the Shannon energy was computed, followed by its envelope, thus retrieving the locations of the signal where energy concentration is higher; that is, where the QRS complexes are, as carried out in [28,29]. The envelope was computed using a moving root mean square (RMS), with a length of 70 samples that was also normalized. The envelope was further transformed into a squared signal. Finally, the filtered signal was multiplied by the obtained square signal, and the R-peaks were detected using scipys's [30] findpeaks function, using a minimum distance of 120 samples and a minimum height of 0.15.

Finally, the metrics of HRV were computed, all based on the time-series of the distance between consecutive R peaks—the RR intervals. These include standard deviation of the RR intervals (SDRRi), square root of the mean sum of the square differences between RR intervals (RMSSD) [31], and SD1 and SD2, extracted from the Poincaré plot (plot of the current RR intervals against the previous ones) [32]. Moreover, the cardiovascular load indicators were extracted from these signals, based on reserve HR (maximum HR—resting HR) including RHR, cardiovascular strain (CVS), and cardiovascular load (CVL), since they have already been used to evaluate the cardiovascular response in the occupational context [33].

2.5.2. Respiratory Inductance Plethysmography

RIP is a non-invasive method of monitoring pulmonary function. By placing elastic bands with embedded coils around the RC and ABD walls, the output is proportional to the variation of the cross-sectional area of the surfaces surrounded by those bands [23,34].

The respiratory signals were first denoised with a finite response band-pass filter with cut-off frequencies of 0.15 and 0.45 Hz [19]. To be able to separate the actual signal in the low frequency band from the tissue artifacts in the high-frequency band and ambient noise in all frequency bands, the signal was further decomposed with masked sift empirical mode decomposition (EMD). EMD is a processing method that is able to decompose nonlinear signals with multiple components into intrinsic mode functions (IMF's), containing a defined frequency and amplitude through the Hilbert Transform [35,36]. When signals are very noisy, traditional EMD is not able to correctly separate components of different time scales, leading to mode-mixing. One of the proposed methods to solve this is injecting a masking signal into the original, preventing lower frequency components from contaminating the wrong IMF [36]. The signal was reconstructed with only IMF 4 as it presented the clearest respiratory pattern. Both signals from the RC and ABD belt were subjected to this procedure.

From the filtered signal, respiratory rate (RR) in breaths per minute was determined through differentiation of the signal and determining its zero-crossings [37]. RC percentage (RC%) is defined as the RC's contribution to tidal volume as a percentage of the sum of both RC and ABD volume variation [38]. The correlation between RC and ABD signals

was determined using a rolling window [39] of 400 samples. Finally, phase synchrony (PS) between the two signals from each belt was determined by applying the Hilbert transform to both signals, extracting the imaginary part (phase) from each of them, and finally, subtracting their imaginary parts [19].

2.5.3. Accelerometer

To denoise the ACC data both from the triaxial ACC mounted on the center of the lower back and from the ACCs in the MuscleBAN devices, a band-pass filter with cut-off frequencies of 0.1 Hz and 10 Hz was used [19,40]. Next, the signals were smoothed with a window of 0.2 s.

Table 1 sums up the extracted metrics from both ECG and RIP metrics.

Table 1. Extracted metrics from ECG and RIP signals.

HRV (ms)	CVL (%)	Frequency (bpm)	Synchronization (%)
SDRRi	RHR	ABD RR	Correlation
RMSSD	CVL	RC RR	Phase Synchrony
SD1	CVS		RC
SD2			

HRV—heart rate variability; SDRRi—standard deviation of consecutive RR peak intervals; RMSSD—root mean square of the consecutive RR peak intervals; RHR—relative heart ate; CVS—cardiovascular strain; CVL—cardiovascular load; SD1—Poincaré plot standard deviation perpendicular to the line of identity; SD2—Poincaré plot standard deviation along the line of identity; ABD—abdominal; RC—rib cage; RR—respiratory rate.

2.6. Signal Segmentation

To be able to identify the different workload volumes of the studied workstations, the work cycles were determined through the ACC data.

2.6.1. Signal Synchronization

The synchronization task (i.e., the 10 jumps) was performed at the same phase of the collection session, ensuring the same initial conditions for all participants. The first step was to match the sampling frequencies of the signals from the MuscleBANs with the ones acquired with the Hub by downsampling the first ones to 350 Hz. Following this, the alignment of the signals acquired by the 3 devices (HUB, Trapezius MuscleBAN, and Bicep MuscleBAN) was performed by initially choosing the ACC axis where the jumping motion was most evident and, finally computing the full cross-correlation, thus determining the dephasing between them [41].

2.6.2. Cycle Detection

To segment the recorded signals, the self-similarity matrix (SSM) [42] was applied, a method that consists of transforming the signal into a feature vector using a sliding window of size w with an overlap of o. The resulting matrix has a shape of n features by m subsequences of the signal ($m = (N - w)/o$), N is the length of the time-series [43]. This method was chosen as some conditions could not be controlled by investigators; for example, line stops and bathroom breaks. Furthermore, it was only possible to videotape the first cycles of the tasks, and time stamps for the start and end of the cycle were not possible to acquire.

To accomplish this, multiple steps were followed:

1. Signal selection and downsampling: the appropriate accelerometer signal was chosen by identifying which axis (x, y, or z) of the three ACC sensors (back, biceps, or trapezius) represented the cyclic nature of the work task in the best way. Downsampling of the chosen signal to the frame rate of the camera was also accomplished.
2. Feature extraction: feature extraction from the signal, namely, peak to peak distance, absolute energy, mean, standard deviation (SD), autocorrelation, traveled distance, kurtosis, and skewness of the signal, was computed with TSFEL [44]. The window

(w) and overlap (o) sizes for each workstation and subject had to be adapted manually. H1: $w \in [50,120]$ samples, $o = 5\%$; H2: $w \in [100,150]$ samples, $o \in [1,5]\%$; H3: $w \in [25,40]$, $o \in [5,10]\%$.

3. SSM computation: a z-normalization of the feature series (row-wise normalization) and a further z-normalization of the windows (column-wise) was performed. SSM computation was carried out by applying the dot product between the feature matrix's transpose by itself (cosine distance between each segment of the feature matrix) [42].
4. Self-similarity function: a column-wise sum of features that enhance parts of the signal with similar structure [42] was made.
5. Anomaly and cycle detection: thresholding the self-similarity function and detecting its fiducial points were carried out [45].
6. Confirmation: synchronization of the signals and video by the last detected jump was performed. Comparison of the positions from the last step with annotations on the video were carried out.

These are presented in Figure 4, where the illustrated recording presents an extended pause of activity, which is excluded from the analysis.

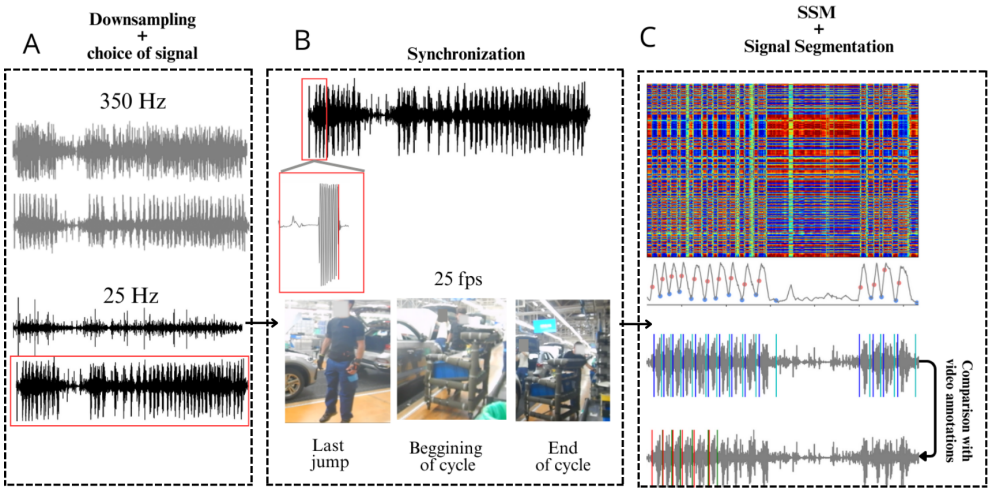


Figure 4. Steps followed to segment data. (**A**)—Visualization of multiple signals and choice of the most cyclic patterned one with its subsequent downsampling to the camera's frame rate. (**B**)—Signals and video synchronization by identifying the last jump in both signal and video. (**C**)—Computation of the SSM and the self-similarity function, thresholding, and finding fiducial points to segment the signal, at last, compared with the video annotations.

2.6.3. Data Cleaning

The signals and location of fiducial points were resampled back to the signal's 350 Hz. To ensure that the time-series could be compared, all of them were cut from the first detected work cycle to the last. Like this, the jumps and end of acquisition information were deleted, leaving the recordings with 40 min.

2.7. Statistical Analysis

Each of the workstations had characteristic movements and cycle times, and to find out if there were statistically significant differences between them over the entire signal duration, a Kruskall–Wallis Test was performed, and for further analysis, the Dunn test was applied.

To evaluate the cardiorespiratory response to workload volume through the signal acquisition, and verify if there was any match with the ER rank associated with the tasks, the metrics mentioned previously were extracted from the time series at two moments: the first and last 10 min of the recordings.

A factorial design (group vs. phase) was used, analyzing the data with the mixed ANOVA test. As the obtained sample did not have an equal distribution of workers, neither

in terms of workstations nor in ergonomic risk rank, and to guarantee a more robust test, avoiding effect-size limitations, the sample size was increased to balance the minority workstations. This balancing was made through an artificial sample generating algorithm, Synthetic Minority Over-sampling TEchnique (SMOTE) [46].

For further reliability, the statistical test was repeated 500 times with a different random seed for the sample generation such that the final result equaled the harmonic mean of the *p*-values [47].

The Yeo–Johnson power transform [48] and the Welch correction were applied to the results when there were violations of the normality and of the equality of variance principles, respectively. The chosen level of significance was 5%, and the post hoc test was the Tukey test. All of the statistical tests were accomplished with the pingouin python (version 0.5.3, Raphael Vallat, CA, USA) package [49] and the JASP computer software (version 0.18, JASP Team, Amsterdam, The Netherlands) [50].

3. Results

In this section, three dimensions of the assembly-line job are presented: (1) workload volume, (2) cardiorespiratory response to workload volume, and (3) cardiorespiratory matching with ER.

3.1. Workload Volume

The workload volume was determined by the duration of one cycle and by the number of cycles performed per 10 min for the entire 40 min of acquisition. A Kruskall–Wallis test was performed on those variables and revealed significant differences for both, as can be verified in Table 2, along with their values.

Table 2. Cycle duration in minutes and number of cycles per 10 min for each workstation.

Variable	H1	H2	H3	*p*	η^2
Cycle Time (min)	2.8 ± 0.5	4.5 ± 0.8	1.1 ± 0.1	0.002 *	3.195
Cycles/10 (min^{-1})	3.4 ± 0.5	2.2 ± 0.2	7.5 ± 0.4	0.002 *	3.214

η^2—eta squared. *—significant results with *p*-value below 5%.

The Dunn post hoc test is represented in Figure 5, showing that statistically there is a distinction between the H2 and H3 workstation's workload volume attributes.

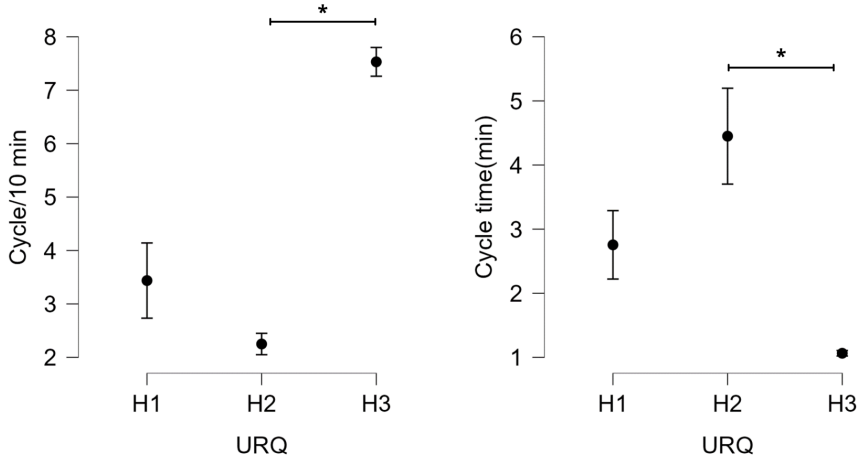


Figure 5. Results from the Dunn post hoc comparisons for the volume metrics. The * indicates a statistically meaningful result. URQ: Workstation.

3.2. Cardiorespiratory Response to Workload Volume

To evaluate cardiac response to the workload volumes endured at each workstation, The cardiovascular load parameters based on RHR and HRV indicators were extracted from the ECG signals. Table 3 shows the 500 simulation results of the mixed ANOVA tests.

In terms of respiration, quantification of the ABD and RC movement frequency and coordination was accomplished, having the results of their factorial analysis exposed in Table 4.

Significant results were submitted to Tukey's post hoc analysis. These revealed that the H2 station had a significantly lower HR in the last when compared with the initial 10 min of monitoring ($p = 0.018$). H3 had significantly lower SDRRi, HR CV ($p = 0.006$), SD RHR ($p = 0.005$), and SD2 ($p = 0.001$). It was also unveiled that through the duration of the acquisition, the H1's cardiac values remained practically constant, as can be seen in Figure 6.

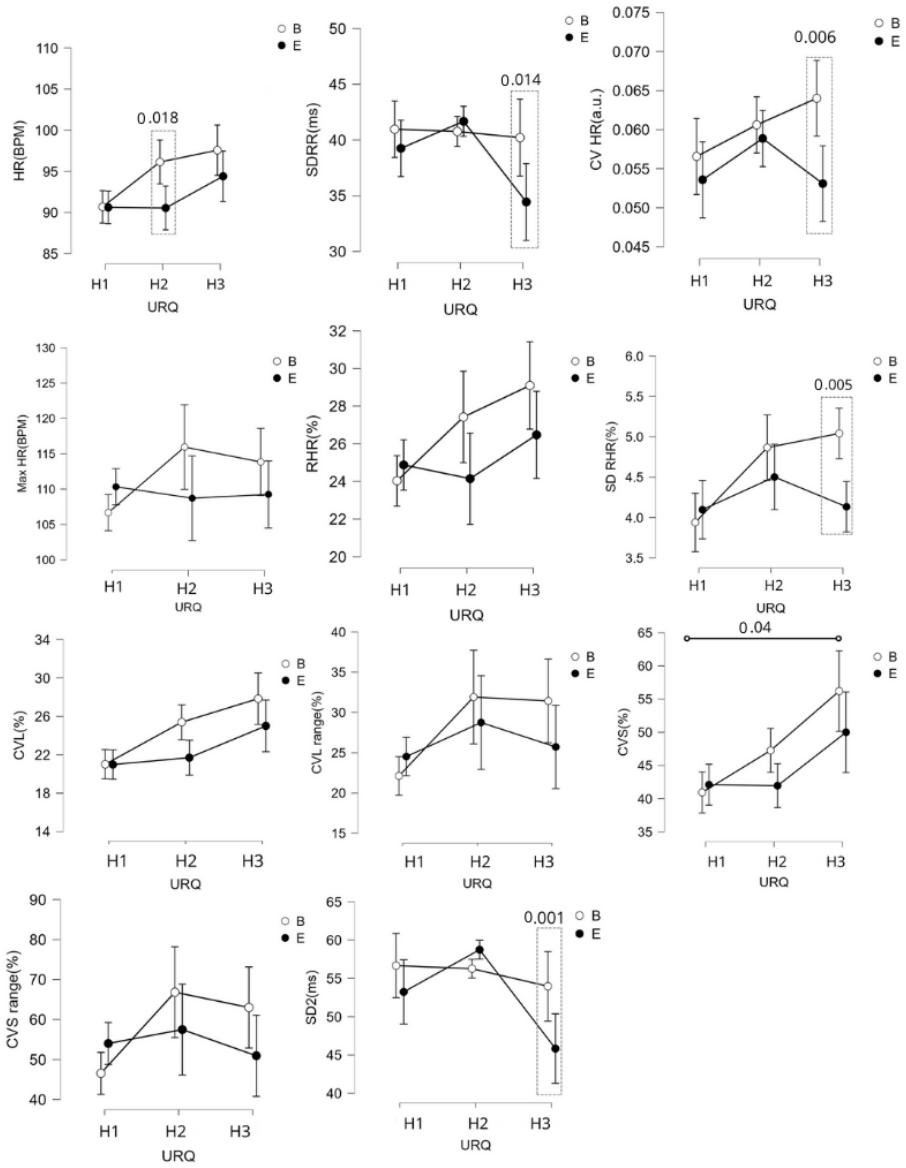


Figure 6. Descriptive plots with Tukey test results for the significant cardiac variables. URQ: Workstation; H1—medium cycle station; H2—long cycle station; H3—short cycle station; B: beginning; E: ending. The dashed line box represents a significant result in the within factor. The solid line represents significant differences in the between factors, with markers on its tips: B—circle; E—solid circle.

Table 3. Mixed ANOVA results from the 500 simulations on the cardiovascular metrics.

Variables	Group						p_g	η_p^2	$p_p h$	η_p^2	p_{int}	η_p^2
	H1		H2		H3							
	B	E	B	E	B	E						
HR (bpm)	90.7 ± 15.5	90.6 ± 16.6	96.2 ± 10.4	90.6 ± 5.9	97.6 ± 13.4	94.4 ± 15.0	0.432	0.040	0.006 *	0.261	0.043 *	0.225
Max HR (bpm)	106.7 ± 18.4	110.3 ± 16.1	116.0 ± 19.4	108.7 ± 9.7	113.9 ± 15.5	109.3 ± 20.8	0.486	0.001	0.097	0.071	0.038 *	0.224
Min HR (bpm)	71.2 ± 14.8	71.7 ± 12.6	73.1 ± 3.5	71.7 ± 5.7	74.6 ± 11.3	76.5 ± 11.7	0.613	0.020	0.793	<0.001	0.406	0.073
HR range (bpm)	29.7 ± 6.8	34.2 ± 8.5	41.4 ± 8.5	35.9 ± 6.2	39.3 ± 11.5	32.7 ± 10.6	0.155	0.094	0.179	0.001	0.053	0.219
SDRR (ms)	41.0 ± 14.0	39.0 ± 11.0	41.0 ± 8.0	42.0 ± 8.0	40.0 ± 12.0	34.0 ± 7.0	0.530	0.025	0.018 *	0.192	0.009 *	0.349
RMSSD (ms)	19.0 ± 5.0	17.0 ± 8.0	24.0 ± 7.0	25.0 ± 7.0	24.0 ± 15.0	22.0 ± 12.0	0.123	0.129	0.424	<0.001	0.445	0.054
CV HR	6.0 ± 2.0	5.0 ± 1.0	6.0 ± 1.0	6.0 ± 1.0	6.0 ± 2.0	5.0 ± 1.0	0.273	0.043	0.001 *	0.318	0.017 *	0.282
RHR (%)	24.0 ± 6.0	24.9 ± 6.5	27.4 ± 6.4	24.2 ± 2.7	29.1 ± 6.6	26.5 ± 6.8	0.229	0.075	0.001 *	0.268	0.021 *	0.269
Max RHR (%)	32.5 ± 11.1	35.3 ± 0.0	51.8 ± 19.0	42.5 ± 8.2	42.4 ± 9.2	39.0 ± 12.5	0.309	0.027	0.090	<0.001	0.055	0.179
Min RHR (%)	9.9 ± 3.9	9.3 ± 1.4	9.4 ± 0.3	8.5 ± 2.5	9.4 ± 3.4	11.1 ± 4.9	0.474	0.041	0.777	<0.001	0.345	0.083
RHR range (%)	28.8 ± 9.9	31.4 ± 8.5	35.2 ± 14.5	31.9 ± 5.0	33.0 ± 10.2	27.9 ± 10.6	0.196	0.001	0.175	<0.001	0.074	0.184
SD RHR (%)	3.9 ± 1.3	4.1 ± 1.0	4.9 ± 1.4	4.5 ± 0.8	5.0 ± 1.4	4.1 ± 1.2	0.274	0.001	0.001 *	0.387	0.030 *	0.241
CV RHR	5.7 ± 1.0	5.9 ± 0.6	5.5 ± 0.7	5.1 ± 0.4	6.0 ± 1.3	6.5 ± 0.7	0.071	0.211	0.563	<0.001	0.007 *	0.361
CVS (%)	40.9 ± 9.9	42.1 ± 6.4	47.3 ± 9.0	41.9 ± 6.6	56.2 ± 14.2	50.0 ± 9.8	0.051	0.213	0.008 *	0.253	0.094	0.174
CVS range (%)	46.6 ± 11.9	54.0 ± 19.1	66.8 ± 26.1	57.5 ± 9.8	63.0 ± 19.6	51.0 ± 11.3	0.133	0.076	0.162	<0.001	0.040 *	0.242
CVL (%)	21.0 ± 4.4	21.0 ± 2.9	25.4 ± 5.3	21.7 ± 3.1	27.9 ± 5.7	25.0 ± 4.8	0.027 *	0.258	0.006 *	0.265	0.058	0.207
CVL range (%)	22.1 ± 5.2	24.5 ± 8.0	31.9 ± 13.9	28.8 ± 5.0	31.4 ± 9.3	25.7 ± 6.5	0.075	0.136	0.198	<0.001	0.040 *	0.241
SD1 (ms)	14.0 ± 6.0	14.0 ± 6.0	18.0 ± 5.0	18.0 ± 5.0	17.0 ± 10.0	15.0 ± 8.0	0.123	0.129	0.424	<0.001	0.445	0.054
SD2 (ms)	57.0 ± 21.0	53.0 ± 16.0	56.0 ± 11.0	59.0 ± 12.0	54.0 ± 15.0	46.0 ± 9.0	0.502	0.035	0.015 *	0.202	0.008 *	0.360

HR—heart rate; SDRRi—standard deviation of RR intervals; RHR—relative heart rate; CVS—cardiovascular strain; CVL—cardiovascular load; SD1—Poincaré plot standard deviation perpendicular to the line of identity; SD2—Poincaré plot standard deviation along the line of identity; Max—maximum; Min—minimum; SD—standard deviation; CV—coefficient of variation; bpm—beats per minute; p_g—harmonic mean combined p-value for the between factor; p_{ph}—harmonic mean combined p-value for the within factor; p_{int}—harmonic mean combined p-value for the interaction; η_p^2—partial eta squared; B—beginning; E—ending; *—significant results with p-value below 5%. All the presented values are dimensionless.

Table 4. Mixed ANOVA results from the 500 simulations on the respiratory metrics.

Variables	Group						p_g	η_p^2	p_{ph}	η_p^2	p_{int}	η_p^2
	H1		H2		H3							
	B	E	B	E	B	E						
RC (bpm)	24.7 ± 1.4	24.4 ± 1.2	26.0 ± 1.0	25.4 ± 0.5	24.5 ± 1.6	24.8 ± 1.2	0.113	0.181	0.504	0.001	0.131	0.136
Max RC (bpm)	63.2 ± 11.5	65.6 ± 9.8	68.2 ± 11.3	54.0 ± 3.2	54.2 ± 5.3	73.4 ± 15.8	0.534	0.031	0.033	0.110	<0.001 **	0.457
Min RC (bpm)	15.2 ± 0.8	13.7 ± 1.3	14.1 ± 0.8	14.9 ± 0.6	14.4 ± 1.9	14.4 ± 0.9	0.891	0.001	0.533	0.001	<0.001 **	0.385
SD RC (bpm)	6.6 ± 1.1	6.3 ± 1.1	6.9 ± 0.7	6.3 ± 0.6	5.9 ± 0.7	6.8 ± 0.9	0.391	0.050	0.491	0.001	0.013	0.315
ABD (bpm)	24.2 ± 0.2	25.0 ± 0.6	25.5 ± 0.3	24.4 ± 0.4	24.5 ± 1.3	24.6 ± 0.9	0.190	0.126	0.468	0.001	<0.001 **	0.458
Max ABD (bpm)	59.3 ± 5.9	59.3 ± 5.5	55.0 ± 3.5	67.2 ± 2.7	56.3 ± 10.8	66.4 ± 11.5	0.697	0.020	<0.001 **	0.365	<0.001 **	0.352
Min ABD (bpm)	14.1 ± 0.4	14.4 ± 0.5	14.0 ± 0.8	13.5 ± 1.4	14.1 ± 0.8	13.8 ± 1.4	0.282	0.056	0.621	0.001	0.694	0.019
SD ABD (bpm)	6.3 ± 0.5	6.1 ± 0.6	6.0 ± 0.5	6.9 ± 0.3	6.3 ± 0.8	6.7 ± 1.1	0.539	0.018	0.008 *	0.260	0.077	0.174
RC (%)	53.3 ± 13.3	54.3 ± 14.3	59.1 ± 1.9	59.1 ± 2.5	55.2 ± 9.7	55.9 ± 8.8	0.423	0.038	0.105	0.079	0.265	0.088
Correlation (%)	40.0 ± 28.0	27.0 ± 38.0	60.0 ± 6.0	48.0 ± 8.0	57.0 ± 17.0	56.0 ± 18.0	0.022 *	0.174	<0.001 **	0.477	0.013 *	0.279
PS (%)	53.0 ± 13.0	43.0 ± 15.0	64.0 ± 3.0	59.0 ± 4.0	64.0 ± 10.0	64.0 ± 10.0	0.044 *	0.158	<0.001 **	0.420	0.015 *	0.263

RC—rib cage respiratory frequency; ABD—abdominal respiratory frequency; Correlation—correlation between rib cage and abdominal breathing; PS—phase synchrony between rib cage and abdominal breathing; Max—maximum; Min—minimum; SD—standard deviation; bpm—breaths per minute; H1—medium cycle station; H2—long cycle station; H3—short cycle station; p_g—harmonic mean combined p-value for the between factor; p_{ph}—harmonic mean combined p-value for the within factor; p_{int}—harmonic mean combined p-value for the interaction; η_p^2—partial eta squared; B—beginning; E—ending; *—significant results with p-value below 5%; **—significant results with p-value below 1%. All the presented values are dimensionless.

When looking at the evolution of the RIP extracted metrics, it is evident that for the H3 workstation, max RC RR increased significantly from the beginning to the end ($p = 0.017$), that its value at the end of acquisition is superior to the one in the H2 station, and that the phase synchrony between respiratory walls is larger than H1's ($p = 0.005$). For the H2 workstation, ABD RR decreased and its MAX and SD increased significantly ($p \in [0.005; 0.040]$). Another notable result was the decrease in correlation for H2 ($p = 0.039$) and in the PS for H1 ($p = 0.039$) ($p < 0.001$) between the respiratory walls movements throughout the data collection, shown in Figure 7.

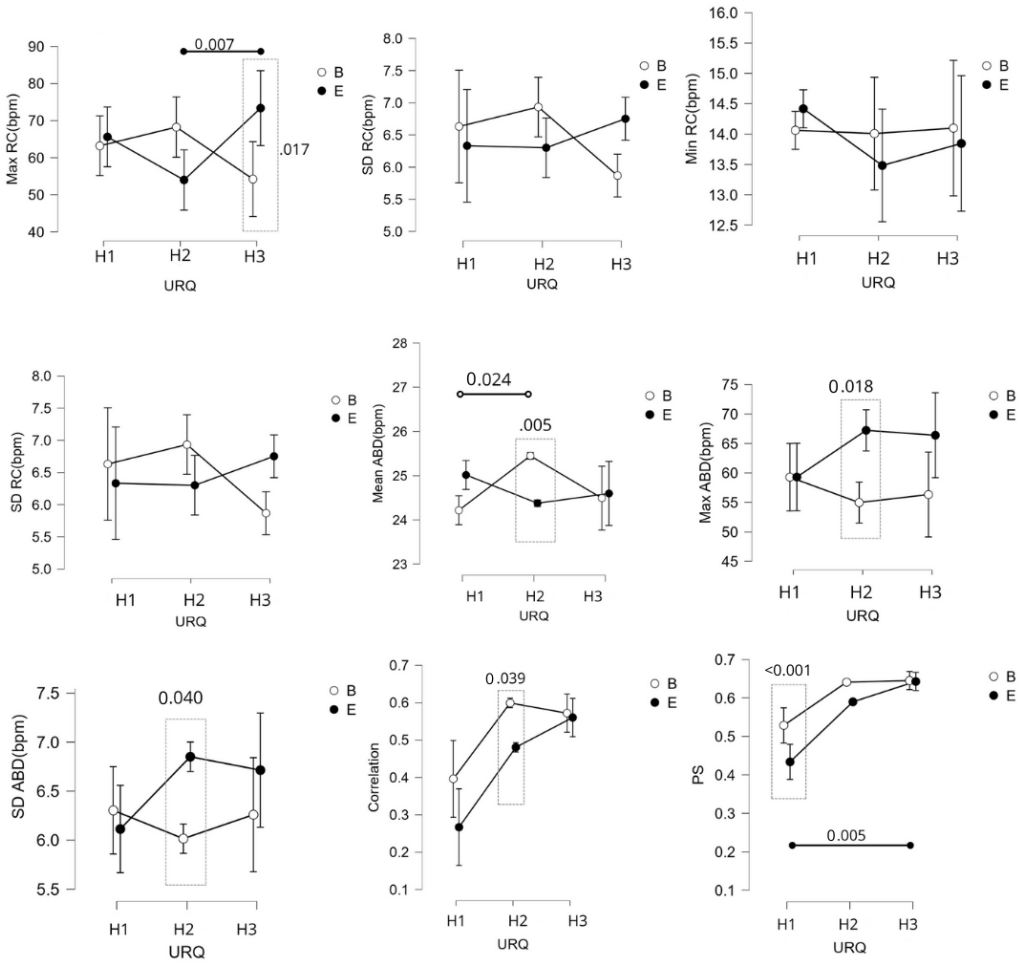


Figure 7. Descriptive plots with the Tukey test results for the significant respiratory variables. URQ: Workstation; H1—medium cycle station; H2—long cycle station; H3—short cycle station; B: beginning; E: ending. The dashed line box represents a significant result in the within factor. The solid line represents significant differences in the between factors, with markers on its tips: B—circle; E—solid circle.

3.3. Cardiorespiratory Response to Ergonomic Risk

The comparative results of the cardiovascular response between ER stratification at the start and the end of the acquisition are shown in Table 5.

The same analysis results but for the respiratory variables can be verified in Table 6.

Table 5. Mixed ANOVA results from the 500 simulations on the cardiovascular metrics for the ergonomic risk stratification.

Variables	Risk Stratification						p_g	η_p^2	p_{ph}	η_p^2	p_{int}	η_p^2
	Low		Moderate		Moderate-High							
	B	E	B	E	B	E						
HR (bpm)	78.7 ± 9.5	76.7 ± 11.2	92.5 ± 13.8	89.0 ± 14.2	99.8 ± 11.5	97.7 ± 10.8	0.001 *	0.429	0.008 *	0.230	0.626	0.008
Max HR (bpm)	86.1 ± 9.5	85.3 ± 13.8	116.5 ± 23.0	112.1 ± 13.7	116.2 ± 13.5	113.2 ± 16.1	0.001 *	0.481	0.088	0.075	0.588	0.005
Min HR (bpm)	66.5 ± 8.5	63.8 ± 8.7	73.3 ± 12.0	71.1 ± 12.4	76.1 ± 10.4	79.4 ± 8.6	0.006 *	0.303	0.631	0.001	0.065	0.213
HR range (bpm)	22.3 ± 2.4	23.7 ± 7.4	38.8 ± 13.3	37.2 ± 4.5	40.1 ± 12.2	33.8 ± 9.2	0.001 *	0.592	0.188	0.001	0.365	0.070
SDRR (ms)	39.0 ± 5.0	39.0 ± 3.0	42.0 ± 11.0	41.0 ± 12.0	38.0 ± 13.0	33.0 ± 7.0	0.115	0.136	0.031 *	0.177	0.071	0.210
RMSSD (ms)	20.0 ± 3.0	22.0 ± 6.0	24.0 ± 7.0	27.0 ± 9.0	22.0 ± 15.0	19.0 ± 11.0	0.429	0.054	0.525	0.001	0.082	0.176
CV HR	0.1 ± 0.0	0.1 ± 0.0	0.1 ± 0.0	0.1 ± 0.0	0.1 ± 0.0	0.1 ± 0.0	0.008 *	0.335	0.003 *	0.299	0.098	0.154
RHR (bpm)	20.3 ± 5.0	18.7 ± 5.4	30.8 ± 7.6	26.3 ± 5.4	29.5 ± 6.9	27.6 ± 6.1	0.003 *	0.373	0.009 *	0.222	0.580	0.008
Max RHR (bpm)	28.7 ± 6.0	28.2 ± 7.5	43.5 ± 14.6	40.9 ± 6.8	43.3 ± 9.5	41.0 ± 10.6	0.001 *	0.432	0.097	0.050	0.438	0.004
Min RHR (bpm)	9.3 ± 4.1	9.2 ± 1.5	9.7 ± 1.6	8.2 ± 2.0	8.8 ± 3.0	11.6 ± 4.9	0.553	0.023	0.766	0.001	0.078	0.208
RHR range (bpm)	17.3 ± 2.1	16.3 ± 5.9	35.5 ± 14.1	33.9 ± 5.0	34.5 ± 9.8	29.4 ± 8.9	0.001*	0.615	0.211	0.014	0.347	0.072
SD RHR (bpm)	3.0 ± 0.5	2.9 ± 0.7	5.4 ± 0.9	4.9 ± 0.6	5.2 ± 1.4	4.4 ± 0.9	0.001 *	0.618	0.001 *	0.361	0.038 *	0.194
CV RHR (bpm)	6.3 ± 0.9	6.2 ± 0.6	5.2 ± 0.4	5.3 ± 0.6	5.9 ± 1.2	6.4 ± 0.7	0.001 *	0.447	0.534	0.001	0.065	0.210
CVS	58.9 ± 14.6	46.0 ± 4.6	54.0 ± 10.1	46.7 ± 5.1	52.3 ± 13.9	48.8 ± 11.8	0.690	0.002	0.005 *	0.241	0.584	0.014
CVS range (bpm)	42.9 ± 6.5	44.1 ± 6.8	63.9 ± 18.6	65.6 ± 14.0	62.1 ± 22.4	51.0 ± 11.3	0.010 *	0.328	0.156	0.001	0.405	0.061
CVL (bpm)	21.3 ± 6.5	20.3 ± 2.7	25.0 ± 4.8	23.0 ± 1.3	26.9 ± 6.3	25.1 ± 5.4	0.103	0.143	0.006 *	0.240	0.631	0.011
CVL range (bpm)	18.7 ± 2.1	20.5 ± 4.9	34.6 ± 10.6	32.9 ± 5.3	31.8 ± 10.3	26.4 ± 5.8	0.001 *	0.531	0.187	0.001	0.399	0.058
SD1 (ms)	14.0 ± 2.0	15.0 ± 4.0	18.0 ± 5.0	16.0 ± 6.0	16.0 ± 11.0	13.0 ± 8.0	0.429	0.054	0.526	0.001	0.082	0.176
SD2 (ms)	56.0 ± 9.0	54.0 ± 5.0	61.0 ± 19.0	58.0 ± 18.0	51.0 ± 15.0	44.0 ± 8.0	0.086	0.156	0.024 *	0.187	0.113	0.169

HR—heart rate; SDRR—standard deviation of RR intervals; RMSSD—root mean square of successive RR interval differences; RHR—reserve heart rate; CVS—cardiovascular strain; CVL—cardiovascular load; SD1—Poincaré plot standard deviation perpendicular to the line of identity; SD2—Poincaré plot standard deviation along the line of identity; Max—maximum; Min—minimum; SD—standard deviation; p_g—harmonic mean combined *p*-value for the between factor; p_{ph}—harmonic mean combined *p*-value for the within factor; p_{int}—harmonic mean combined *p*-value for the interaction. η_p^2—partial eta squared. *—significant results with *p*-value below 5%. All the presented values are dimensionless.

Table 6. Mixed ANOVA results from the 500 simulations on the respiratory metrics for the ergonomic risk stratification.

Variables	ER						p_g	η_p^2	p_{ph}	η_p^2	p_{int}	η_p^2
	Low		Moderate		Moderate-High							
	B	E	B	E	B	E						
RC (bpm)	23.8 ± 0.4	24.3 ± 0.9	25.8 ± 1.5	25.0 ± 1.0	24.5 ± 1.6	24.9 ± 1.2	0.008*	0.340	0.725	0.001	<0.001 **	0.529
Max RC (bpm)	57.9 ± 13.8	60.6 ± 3.3	66.3 ± 11.6	61.6 ± 10.9	54.1 ± 5.4	72.1 ± 17.0	0.407	0.001	**0.035**	0.100	**0.010**	0.325
Min RC (bpm)	15.2 ± 0.3	14.9 ± 0.3	13.8 ± 0.9	14.3 ± 1.4	14.4 ± 1.8	14.4 ± 0.9	0.052	0.227	0.683	0.001	0.465	0.025
SD RC (bpm)	6.3 ± 1.4	5.4 ± 0.1	6.9 ± 0.6	6.5 ± 0.8	6.0 ± 0.6	6.9 ± 0.7	<0.001 **	0.354	0.547	0.001	<0.001**	0.431
ABD (bpm)	24.3 ± 0.2	24.8 ± 0.7	25.2 ± 0.8	24.9 ± 0.3	24.6 ± 1.3	24.4 ± 0.9	0.147	0.155	0.714	0.001	0.103	0.146
Max ABD (bpm)	62.7 ± 8.6	58.2 ± 5.7	56.3 ± 5.8	66.5 ± 5.5	54.5 ± 8.3	67.0 ± 11.6	0.885	0.001	<0.001 **	0.265	<0.001 **	0.417
Min ABD (bpm)	13.7 ± 0.3	14.6 ± 0.7	14.1 ± 0.7	14.5 ± 0.4	14.1 ± 0.8	13.3 ± 1.4	0.028 *	0.263	0.166	0.054	0.009 *	0.349
SD ABD (bpm)	5.9 ± 0.4	5.6 ± 0.0	5.9 ± 0.5	6.7 ± 0.2	6.4 ± 0.8	6.9 ± 1.0	0.006 *	0.375	0.021 *	0.203	0.008 *	0.338
RC (%)	60.2 ± 13.3	61.5 ± 13.8	57.1 ± 7.8	58.6 ± 8.1	55.9 ± 9.4	56.2 ± 8.8	0.487	0.043	0.042 *	0.151	0.458	0.061
Correlation (%)	63.0 ± 15.0	61.0 ± 24.0	53.0 ± 22.0	34.0 ± 31.0	54.0 ± 15.0	50.0 ± 16.0	0.040	0.153	<0.001 **	0.301	<0.001 **	0.326
Phase Synchrony (%)	72.0 ± 7.0	73.0 ± 11.0	59.0 ± 14.0	53.0 ± 16.0	62.0 ± 8.0	61.0 ± 9.0	0.025	0.195	0.016	0.198	0.025	0.223

RC—rib cage respiratory frequency; ABD—abdominal respiratory frequency; RC (%)—percentage of rib cage contribution to respiration; Correlation—correlation between rib cage and abdominal breathing; PS—phase synchrony between rib cage and abdominal breathing; p_g—harmonic mean combined p-value for the between factor; p_{ph}—harmonic mean combined p-value for the within factor; p_{int}—harmonic mean combined p-value for the interaction. η_p^2—partial eta squared. *—significant results with p-value below 5%; **—significant results with p-value below 1%. All the presented values are dimensionless.

After being submitted to the Tukey post hoc test, and by interpreting the descriptive plot in Figure 8, the moderate–high-risk activities had significantly reduced the SDRRi ($p = 0.037$) and CV of HR ($p = 0.032$). There were significant differences between the low and moderate–high-risk tasks in HR, its maximum, range, RHR range, and CVL range ($p \in [0.004; 0.042]$). Differences among low-risk and moderate-risk were found in maximum HR, HR range, and its coefficient of variation, RHR range, and CVL range ($p \in [< 0.001; 0.047]$).

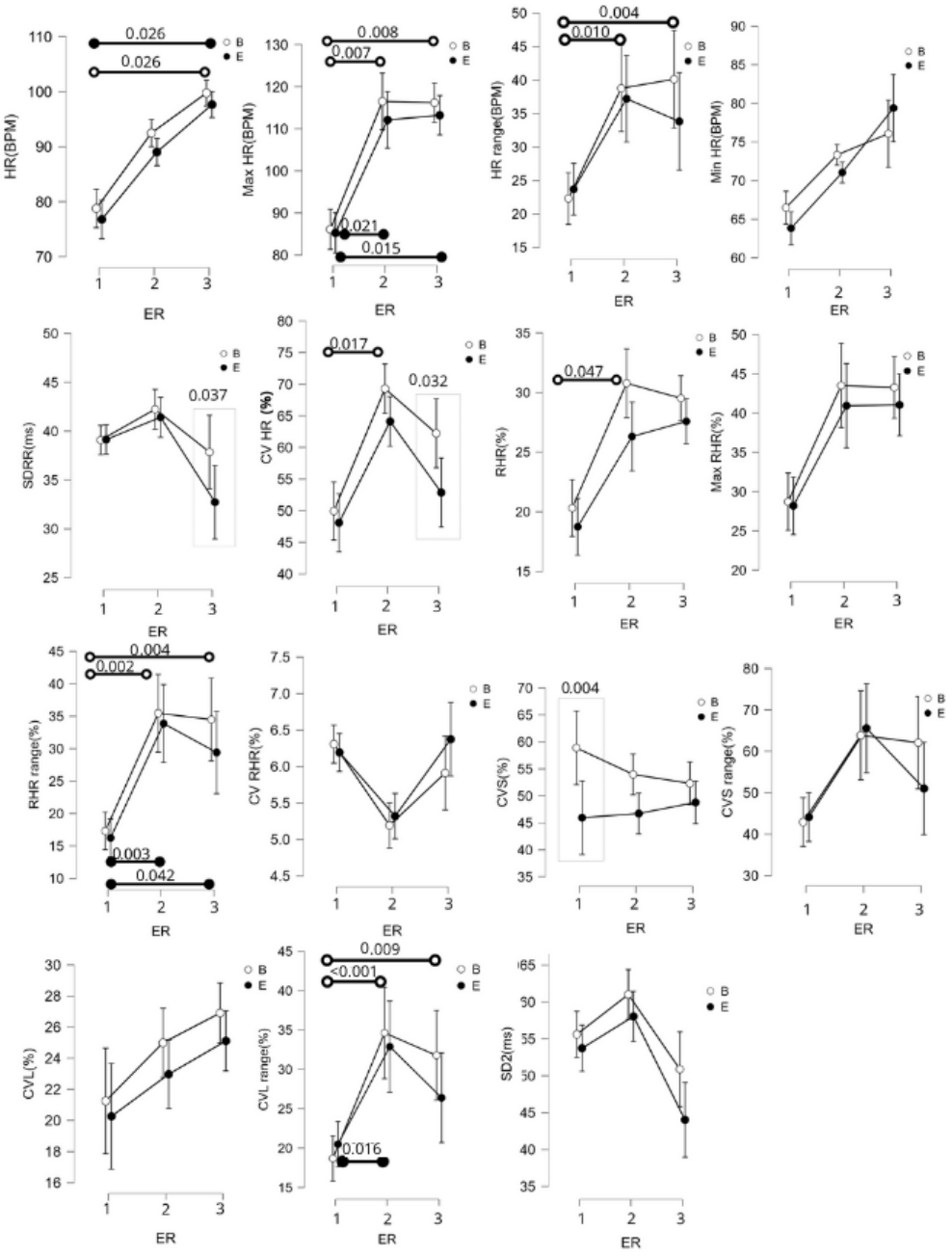


Figure 8. Descriptive plots with the Tukey test results for the significant cardiovascular variables. ER: ergonomic risk stratification; 1: low; 2: moderate; 3: moderate–high; B: beginning; E: ending. The dashed line box represents a significant result in the within factor. The solid line represents significant differences in the between factors, with markers on its tips: B—circle; E—solid circle.

In Figure 9, significant distinctions are shown between the moderate- and low-risk tasks in the mean RC RR, in ABD RR SD, and in PS ($p \in [0.012; 0.036]$). Between the moderate and high risk tasks, there was only a discrepancy in minimum ABD frequency ($p = 0.036$). The low-risk had significantly higher SD of RC RR, SD of ABD RR, and lower minimum ABD RR than of the moderate–high-risk rank ($p \in [0.001; 0.026]$).

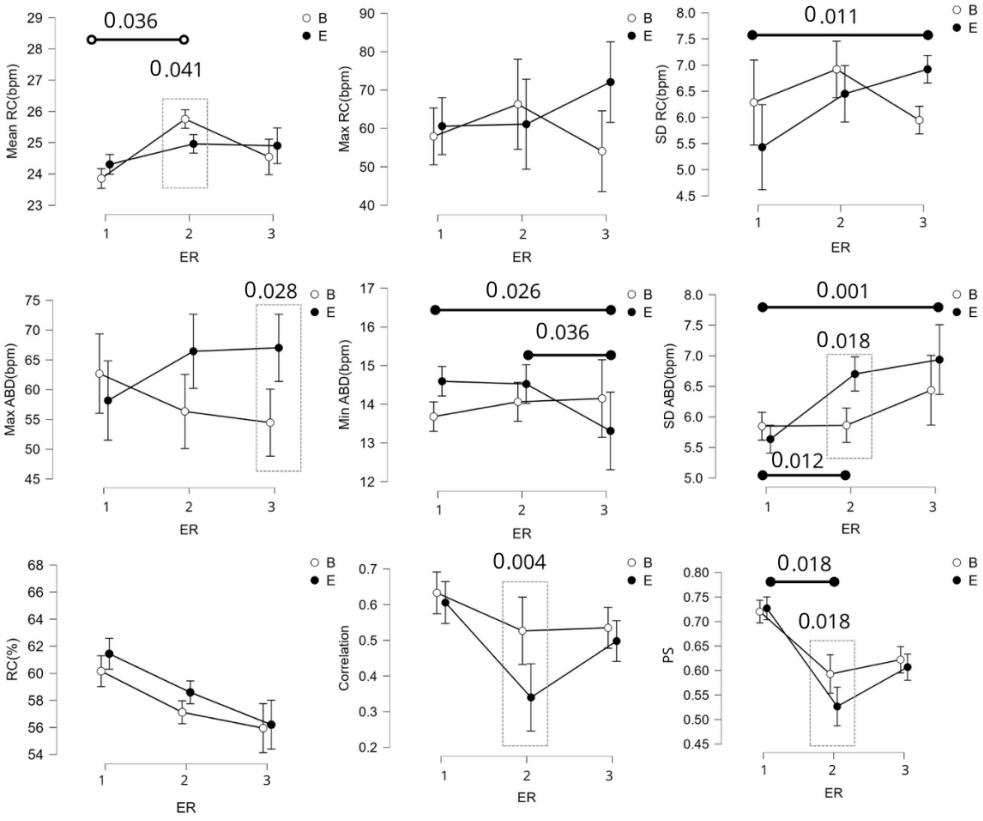


Figure 9. Descriptive plots with the Tukey test results for the significant respiratory variables. ER: ergonomic risk stratification; 1: low; 2: moderate; 3: moderate–high; B: beginning; E: ending. The dashed line box represents a significant result in the within factor. The solid line represents significant differences in the between factors, with markers on its tips: B—circle; E—solid circle.

4. Discussion

This study aimed to investigate the acute response of operators' cardiorespiratory systems to different workload volumes on a real automobile assembly line. Further analysis was conducted to determine the association of this response with occupational risk. Three workstations with different workload volumes were considered: H1, H2, and H3, with medium, long, and short cycles, respectively. The tasks performed at H1 aim to attach the taillights involving arm movements in front of or along the upper body. At H2, workers perform the alignments, which requires upper body bending and applying body weight onto the car. To mount the final pieces of the vehicle, H3 entails multiple overhead movements.

The ECG, RIP, and ACC signals of these volunteer workers were tracked during their shifts. Metrics based on HR (cardiovascular load and variability) and on the resulting breathing patterns (respiratory frequency and respiratory wall coordination) were extracted to quantify the cardiorespiratory effort put into the tasks. These were analyzed at two moments: first and last 10 min of the 40 min recordings. The results of this study yielded a decrease in HRV variables throughout the acquisition time for the H3 station and for the moderate–high ER rank. The cardiovascular response of the H1 workstation did not significantly change during the monitored period. As the tasks progressed, the H2 workstation and the moderate ER rank had a significant increase in the variation of ABD

motion and a decrease in respiratory wall coordination. At the H1 workstation, a decrease in phase synchrony between the thoracic and abdominal walls was verified.

4.1. Cardiovascular Response

HR is an important indicator of the cardiac system state. It can be measured through the ECG, by determining the distance in time between two QRS complexes [51]. This parameter can indicate abnormalities in the electrical activity of the heart, specifically in its rhythm [24]. For instance, when the time between two consecutive beats is too long, this may indicate bradycardia; when it is too short, tachycardia, conditions that may be associated with underlying disease [52]. In addition to being an indicator of disease, HR is used in exercise recommendations. By determining a target HR, the intensity of exercise can be controlled [53].

HRV reflects the balance between the parasympathetic and sympathetic branches of the autonomic nervous system, the regulatory function of the respiratory sinus arrhythmia on HR, and baroreceptor sensitivity (regulation of blood pressure) [32]. The sympathetic activity increases in response to stressful situations and exercise, whereas parasympathetic activation is dominant in resting conditions, maintaining and conserving energy and regulating basic body functions. Specifically, sympathetic stimulation increases HR and force of contraction, while parasympathetic stimulation does the opposite [54]. Therefore, the parasympathetic branch dominates at rest and moderate exercise, giving way to increased HRV [55].

Diminished HRV has been previously linked to fatigue [56], disease [57], and increased mortality [58]. Moreover, fast paced tasks lead to lower decision flexibility, a condition previously connected to higher blood pressure [7]. Furthermore, in a previous study, faster repetitions of lower body resistance training (with time under tension matched with effort) provoked higher volume load, cardiovascular and metabolic strain, and perceived exertion [59]. Workers at H3 experience significant reductions in HRV, pointing to increased cardiovascular stress and potential fatigue, likely due to having the most frequent tasks, i.e., shorter cycles.

The ER score generally agrees with the physiological response. Low-risk tasks have a smaller cardiac load than both moderate- and moderate–high-risk tasks. The last two are distinguished by HRV, since the first ones present a significant reduction in SDRRi throughout the recordings. A possible explanation for this reduction only in high–moderate tasks is that they rely on a long time with arm movements above the head, a work posture that has been associated with considerable circulatory load [60]. The fact that moderate and moderate–high ranks can be discriminated by this metric opens the possibility of better quantifying and separating the intermediate zones of the EAWS score.

Furthermore, it is expected that when HR increases, HRV decreases and vice-versa [61]. Despite that, in the H3 workstation and moderate–high-risk activities, HR is maintained, whereas its variability decreases.

4.2. Respiratory Response

Quiet breathing yields nearly constant frequency and pattern, or when metabolic demands increase, a rise in these parameters is expected [62]. The movements of both RC and ABD walls are mediated by the respiratory muscles: the diaphragm (inspiration), the intercostal muscles (inspiration and expiration), abdominal muscles (mainly expiration), and accessory muscles of respiration [63]. When the movements of these muscles are not matched in time, it may indicate increased work of breathing [64], respiratory muscle fatigue [19,65], or even neuromuscular disease [38,66].

The assembly line processes depend on various arm movements, as can be seen in Figure 1. Considering that solely through arm elevation, metabolic and ventilatory demands have been demonstrated to rise [67], it was expected that these tasks would increase workers' respiratory strain. Moreover, these movements rely on muscles of the rib cage that stabilize arm position and posture [68,69], diminishing their contribution

to respiration, leading the diaphragm and ABD muscles to compensate to keep up with physiological requirements. The previous research on diaphragm activity demonstrated that it contracts not just during respiration but also when fast repetitive changes in posture and limb position occur, to raise ventilatory pressures [70].

As can be seen in Figure 7, at H1, decreased phase synchrony between thoracic and abdominal movements suggest respiratory distress, likely associated with the movements performed near to the upper body demanded by its tasks. H2 shows similar distress, with a marked increase in abdominal motion variation and reduced respiratory wall coordination, indicating a mismatch in muscle effort during respiration, likely due to the bending and weight application required by these tasks. The drop in coordination metrics of the respiratory walls of tasks involving arm movements was also found in Celli et al. for some of the studied subjects. For these, exercise tolerance decreased drastically [69]. In Silva et al., the subjects were put through a fatigue-inducing protocol and also exhibited respiratory wall asynchrony [19].

Unlike the other workstations, the subjects at the H3 maintained the coordination between their RC and ABD respiratory movements. Thus, it indicates that these tasks do not cause as much breathing distress as the ones in the other workstations.

The respiratory response by ER rank showed that the moderate risk results point to a rise in the ABD exertion with a decline in RC contribution. Furthermore, the decrease in both measures of thoraco-abdominal coordination indicates a growth in breathing effort from the first to the last 10 min of the recordings.

The results also point to the low-risk activities having a lower effort of breathing when compared to the other ranks. It appears that the tasks of the moderate–high-risk workstations have more controlled respiration, even though they take a larger toll on the cardiac system. Here it is seen that the breathing load is not compatible with the attributed risk rank. It also gives us another relevant characteristic to discriminate these two ranks.

4.3. Practical Implications

The findings of this study support the incorporation of health monitoring systems on assembly lines, such as wearables, pointing to the most important parameters to be monitored in real-time. These systems could provide critical data to be used in the adjustment of workloads, task rotation, or prompt breaks to manage fatigue and reduce long-term health risks. For instance, reports of the workers' general status could be sent to the occupational physician and alert workers and supervisors of any alarming situation. In the construction industry, some studies have already included this type of monitoring, determining task demand by resorting to respiratory measures [71]. Additionally, alert systems based on HRV were implemented to activate when signs of fatigue were detected, thereby informing supervisors that workers required a break [72]. Regarding ergonomic intervention, these measurements could be used to leverage risk quantification tools, making them more comprehensive of the various domains affecting workers, not only accounting for biomechanical risks.

4.4. Limitations and Future Work

The future studies should consider factors such as worker's experience, time of day, i.e., moment of the shift (morning/afternoon, before/after lunch), as these may influence physiological adaptations. Furthermore, sample size should be increased, giving us a broader vision of the factory's population while increasing the statistical power. Another suggestion is the creation of a risk score that includes cardiorespiratory responses and biomechanical risk, giving way to more individual-specific workplace management.

5. Conclusions

The analysis of cardiorespiratory measurements showed that the workstations with characteristic workload volumes have distinct demand and adaptation mechanisms to the tasks. The H3 workstation with the shortest cycle time is the only one that presents a

decrease in HRV measures during the monitored period. Conversely, it is the workstation that puts less stress on the respiratory system. H2, with the longest cycle tasks, and H1, with the medium length cycle, present higher breathing efforts, as the former's ABD and RC correlation and the latter's phase synchrony decline.

When analyzing different ER tasks, the responses through the acquisition displayed marked differences in cardiac variables between the risk ranks, namely, the low-risk activities had lower HR than moderate–high-risk activities, and a lower Max HR and RHR range than moderate and moderate high ranks. In addition, SDRRi was only reduced throughout the acquisition for the moderate–high-risk tasks. This could be used to better discriminate at the transition zone of moderate to high in the ER scale. In addition to that, respiratory distress did not coincide with ER rank. The moderate-risk tasks conveyed the most asynchronous breathing patterns, along with increased ABD SD and Max and reduced RC RR.

The results of this study revealed important information supporting that cardiorespiratory adaptations should be accounted for in occupational settings, giving way to future field studies and potentially aiding decision making on the assembly line organization.

Author Contributions: D.F.: conceptualization, data collection, formal analysis, data curation, writing—original draft, visualization; L.S. and M.D.: conceptualization, methodology, data collection, data curation, writing—review and editing; C.F.: writing—review and editing; P.P.: methodology, data collection, writing—review and editing; H.L.: writing—review and editing; H.G.: conceptualization, supervision, project administration, writing—review and editing, and funding acquisition. All authors have read and agreed to the published version of the manuscript.

Funding: This work was supported by Project OPERATOR (NORTE01-0247-FEDER-045910), cofinanced by the ERDF—European Regional Development Fund through the North Portugal Regional Operational Program and Lisbon Regional Operational Program and by the Portuguese Foundation for Science and Technology, under the MIT Portugal Program (2019 Open Call for Flagship projects). M. Dias and P. Probst were supported by the doctoral Grants SFRH/BD/151375/2021 and RT/BD/152843/2021, respectively, financed by the Portuguese Foundation for Science and Technology (FCT), and with funds from State Budget, under the MIT Portugal Program.

Institutional Review Board Statement: The study was conducted in accordance with the Declaration of Helsinki, and OPERATOR projected procedures were reviewed by the Ethics Committee of University of Porto, as partner of the project, under the approval number reference 2020/09-6.

Informed Consent Statement: Informed consent was obtained from all subjects involved in the study.

Data Availability Statement: The datasets presented in this article are not readily available because of a non-disclosure agreement with the automotive company. Requests to access the datasets should be directed to https://libphys.pt/en/contacts (accessed on 1 April 2024).

Conflicts of Interest: The authors declare no conflicts of interest.

Abbreviations

The following abbreviations are used in this manuscript:

HR	Heart rate
ER	Ergonomic risk
RHR	Relative heart rate
RIP	Respiratory inductance plethysmography
HRV	Heart rate variability
ACC	Accelerometer
ECG	Electrocardiography
EAWS	European Assembly Sheet
SDRRi	Standard deviation of the RR intervals

RMSSD	Square root of the mean sum of the square differences between RR intervals
SD1	Poincaré plot standard deviation perpendicular to the line of identity
SD2	Poincaré plot standard deviation along the line of identity
CVL	Cardiovascular load
CVS	Cardiovascular strain
IMF	Intrinsic mode function
RR	Respiratory rate
PS	Phase synchrony
SSM	Self-similarity matrix

References

1. Eurostat. Hours of Work—Annual Statistics. 2023. https://ec.europa.eu/eurostat/statistics-explained/index.php?title=Hours_of_work_-_annual_statistics&oldid=565451#How_does_the_average_usual_working_week_vary_across_economic_activities_and_occupations.3F (accessed on October 2023).
2. Niu, S. Ergonomics and occupational safety and health: An ILO perspective. *Appl. Ergon.* **2010**, *41*, 744–753. [CrossRef] [PubMed]
3. Lowe, B.D.; Dempsey, P.G.; Jones, E.M. Ergonomics assessment methods used by ergonomics professionals. *Appl. Ergon.* **2019**, *81*, 102882. [CrossRef] [PubMed]
4. Andreas, G.W.J.; Johanssons, E. Observational Methods for Assessing Ergonomic Risks for Work-Related Musculoskeletal Disorders. A Scoping Review. *Rev. Cienc. Salud* **2018**, *16*, 8–38.
5. Samani, A.; Holtermann, A.; Søgaard, K.; Holtermann, A.; Madeleine, P. Following ergonomics guidelines decreases physical and cardiovascular workload during cleaning tasks. *Ergonomics* **2012**, *55*, 295–307. [CrossRef] [PubMed]
6. van der Beek, A.J.; Frings-Dresen, M.H. Assessment of mechanical exposure in ergonomic epidemiology. *Occup. Environ. Med.* **1998**, *55*, 291–299. [CrossRef] [PubMed]
7. Pickering, T.; Devereux, R.; James, G.; Gerin, W.; Landsbergis, P.; Schnall, P.; Schwartz, J. Environmental influences on blood pressure and the role of job strain. *J. Hypertens. Suppl. Off. J. Int. Soc. Hypertens.* **1996**, *14*, S179–S185.
8. Krause, N.; Brand, R.J.; Kaplan, G.A.; Kauhanen, J.; Malla, S.; Tuomainen, T.P.; Salonen, J.T. Occupational physical activity, energy expenditure and 11-year progression of carotid atherosclerosis. *Scand. J. Work Environ. Health* **2007**, *33*, 405–424. [CrossRef] [PubMed]
9. Krause, N.; Arah, O.A.; Kauhanen, J. Physical activity and 22-year all-cause and coronary heart disease mortality. *Am. J. Ind. Med.* **2017**, *60*, 976–990. [CrossRef] [PubMed]
10. Holtermann, A.; Krause, N.; van der Beek, A.J.; Straker, L. The physical activity paradox: Six reasons why occupational physical activity (OPA) does not confer the cardiovascular health benefits that leisure time physical activity does. *Br. J. Sport. Med.* **2018**, *52*, 149–150. [CrossRef]
11. Lunde, L.K.; Koch, M.; Veiersted, K.B.; Moen, G.H.; Wærsted, M.; Knardahl, S. Heavy Physical Work: Cardiovascular Load in Male Construction Workers. *Int. J. Environ. Res. Public Health* **2016**, *13*, 356. [CrossRef]
12. Wu, H.C.; Wang, M.J.J. Relationship between maximum acceptable work time and physical workload. *Ergonomics* **2002**, *45*, 280–289. [CrossRef]
13. Lin, Y.C.; Lin, Y.W. An Index to Assess Overwork-Related Adverse Effects on Employees Under the Occupational Safety and Health Act in Taiwan. *Saf. Health Work* **2022**, *13*, 401–407. [CrossRef] [PubMed]
14. Romero, D.; Stahre, J.; Wuest, T.; Noran, O.; Bernus, P.; Fasth, Fast-Berglund, Å.; Gorecky, D. Towards an Operator 4.0 Typology: A Human-Centric Perspective on the Fourth Industrial Revolution Technologies. In Proceedings of the International Conference on Computers and Industrial Engineering (CIE46), Tianjin, China, 29–31 October 2016.
15. Palmerud, G.; Forsman, M.; Neumann, W.P.; Winkel, J. Mechanical exposure implications of rationalization: A comparison of two flow strategies in a Swedish manufacturing plant. *Appl. Ergon.* **2012**, *43*, 1110–1121. [CrossRef]
16. Kazmierczak, K.; Mathiassen, S.E.; Forsman, M.; Winkel, J. An integrated analysis of ergonomics and time consumption in Swedish 'craft-type' car disassembly. *Appl. Ergon.* **2005**, *36*, 263–273. [CrossRef] [PubMed]
17. Massaroni, C.; Nicolò, A.; Lo Presti, D.; Sacchetti, M.; Silvestri, S.; Schena, E. Contact-Based Methods for Measuring Respiratory Rate. *Sensors* **2019**, *19*, 908. [CrossRef]
18. Louhevaara, V.; Smolander, J.; Aminoff, T.; Korhonen, O.; Shen, N. Cardiorespiratory responses to fatiguing dynamic and isometric hand-grip exercise. *Eur. J. Appl. Physiol.* **2000**, *82*, 340–344. [CrossRef] [PubMed]
19. Silva, L.; Dias, M.; Folgado, D.; Nunes, M.; Namburi, P.; Anthony, B.; Carvalho, D.; Carvalho, M.; Edelman, E.; Gamboa, H. Respiratory Inductance Plethysmography to Assess Fatigability during Repetitive Work. *Sensors* **2022**, *22*, 4247. [CrossRef] [PubMed]
20. Carvalho, D.; Silva, L.; Carvalho, M.; Dias, M.; Costa, N.; Folgado, D.; Nunes, M.; Gamboa, H.; Andza, K.; Edelman, E. Cardiovascular Reactivity (CVR) During Repetitive Work in the Presence of Fatigue. In *Intelligent Human Systems Integration (IHSI 2023): Integrating People and Intelligent Systems*; Ahram, T., Karwowski, W., Bucchianico, P.D., Taiar, R., Casarotto, L., Costa, P., Eds.; AHFE Open Access; AHFE International: New York, NY, USA , 2023; Volume 69. [CrossRef]
21. Otto, A.; Scholl, A. Incorporating ergonomic risks into assembly line balancing. *Eur. J. Oper. Res.* **2011**, *212*, 277–286. [CrossRef]

22. Schaub, K.; Caragnano, G.; Britzke, B.; Bruder, R. The European Assembly Worksheet. *Theor. Issues Ergon. Sci.* **2013**, *14*, 616–639. [CrossRef]
23. Gastinger, S.; Donnelly, A.; Dumond, R.; Prioux, J. A review of the evidence for the use of ventilation as a surrogate measure of energy expenditure. *J. Parenter. Enter. Nutr.* **2014**, *38*, 926–938. [CrossRef]
24. Gholam-Hosseini, H.; Nazeran, H. Detection and extraction of the ECG signal parameters. In Proceedings of the 20th Annual International Conference of the IEEE Engineering in Medicine and Biology Society. Vol. 20 Biomedical Engineering Towards the Year 2000 and Beyond (Cat. No. 98CH36286), Hong Kong, China, 1 November 1998 ; IEEE: Piscataway, NJ, USA, 1998; pp. 127–130.
25. Chen, C.C.; Tsui, F.R. Comparing different wavelet transforms on removing electrocardiogram baseline wanders and special trends. *BMC Med. Inform. Decis. Mak.* **2020**, *20*, 343. [CrossRef] [PubMed]
26. Gurumoorthy, S.; Muppalaneni, N.B.; Kumari, G.S. EEG Signal Denoising Using Haar Transform and Maximal Overlap Discrete Wavelet Transform (MODWT) for the Finding of Epilepsy. In *Epilepsy*; Misciagna, S., Ed.; IntechOpen: Rijeka, Croatia, 2020; Chapter 8. [CrossRef]
27. He, H.; Tan, Y.; Wang, Y. Optimal Base Wavelet Selection for ECG Noise Reduction Using a Comprehensive Entropy Criterion. *Entropy* **2015**, *17*, 6093–6109. [CrossRef]
28. Xu, W.; Du, F. A Robust Qrs Complex Detection Method Based on Shannon Energy Envelope and Hilbert Transform. *J. Mech. Med. Biol.* **2022**, *22*, 2240013. [CrossRef]
29. Beyramienanlou, H.; Lotfivand, N. Shannon's energy based algorithm in ECG signal processing. *Comput. Math. Methods Med.* **2017**, *2017*, 8081361. [CrossRef] [PubMed]
30. Virtanen, P.; Gommers, R.; Oliphant, T.E.; Haberland, M.; Reddy, T.; Cournapeau, D.; Burovski, E.; Peterson, P.; Weckesser, W.; Bright, J.; et al. SciPy 1.0: Fundamental Algorithms for Scientific Computing in Python. *Nat. Methods* **2020**, *17*, 261–272. [CrossRef] [PubMed]
31. Malik, M.; Bigger, J.T.; Camm, A.; Kleiger, R.E.; Malliani, A.; Moss, A.J.; Shwartz, P.J. Heart rate variability Standards of measurement, physiological interpretation, and clinical use. *Eur. Heart J.* **1996**, vol.17 , 354–381. [CrossRef]
32. Shaffer, F.; Ginsberg, J.P. An Overview of Heart Rate Variability Metrics and Norms. *Front. Public Health* **2017**, *5*, 290215. [CrossRef] [PubMed]
33. Dias, M.; Silva, L.; Folgado, D.; Nunes, M.L.; Cepeda, C.; Cheetham, M.; Gamboa, H. Cardiovascular load assessment in the workplace: A systematic review. *Int. J. Ind. Ergon.* **2023**, *96*, 103476. [CrossRef]
34. Allen, J.L.; Greenspan, J.S.; Deoras, K.S.; Keklikian, E.; Wolfson, M.R.; Shaffer, T.H. Interaction Between Chest Wall Motion and Lung Mechanics in Normal Infants and Infants with Bronchopulmonary Dysplasia. *Pediatr. Pulmonol.* **1991**, *11*, 37–43. [CrossRef]
35. Liu, S.; Gao, R.X.; John, D.; Staudenmayer, J.; Freedson, P. Tissue artifact removal from respiratory signals based on empirical mode decomposition. *Ann. Biomed. Eng.* **2013**, *41*, 1003–1015. [CrossRef]
36. Deering, R.; Kaiser, J.F. The use of a masking signal to improve empirical mode decomposition. In Proceedings of the IEEE International Conference on Acoustics, Speech, and Signal Processing (ICASSP'05), Philadelphia, PA, USA, 23–23 March 2005; IEEE: Piscataway, NJ, USA, 2005; Volume 4, pp. 485–488
37. Rétory, Y.; Niedzialkowski, P.; de Picciotto, C.; Bonay, M.; Petitjean, M. New Respiratory Inductive Plethysmography (RIP) Method for Evaluating Ventilatory Adaptation during Mild Physical Activities. *PLoS ONE* **2016**, *11*, e0151983. [CrossRef] [PubMed]
38. Ryan, L.; Rahman, T.; Strang, A.; Heinle, R.; Shaffer, T.H. Diagnostic differences in respiratory breathing patterns and work of breathing indices in children with Duchenne muscular dystrophy. *PLoS ONE* **2020**, *15*, e0226980. [CrossRef] [PubMed]
39. Makowski, D.; Pham, T.; Lau, Z.J.; Brammer, J.C.; Lespinasse, F.; Pham, H.; Schölzel, C.; Chen, S.H.A. NeuroKit2: A Python toolbox for neurophysiological signal processing. *Behav. Res. Methods* **2021**, *53*, 1689–1696. [CrossRef] [PubMed]
40. Lester, J.; Hannaford, B.; Borriello, G. "Are You with Me?"—Using Accelerometers to Determine If Two Devices Are Carried by the Same Person. In *Pervasive Computing. Pervasive 2004*; Ferscha, A., Mattern, F., Eds.; Lecture Notes in Computer Science; Springer: Berlin/Heidelberg, Germany, 2004; Volume 3001, pp. 33–50. [CrossRef]
41. PLUX Biosignals. Device Synchronisation—Cable, Light and Sound Approaches. 2022. Available online: http://notebooks.pluxbiosignals.com/notebooks/Categories/Pre-Process/synchronisation_rev.html (accessed on May 2023).
42. Rodrigues, J.; Liu, H.; Folgado, D.; Belo, D.; Schultz, T.; Gamboa, H. Feature-Based Information Retrieval of Multimodal Biosignals with a Self-Similarity Matrix: Focus on Automatic Segmentation. *Biosensors* **2022**, *12*, 1182. [CrossRef] [PubMed]
43. Paulus, J.; Müller, M.; Klapuri, A. Audio-based music structure analysis. In Proceedings of the 11th International Society for Music Information Retrieval Conference (ISMIR 2010), Utrecht, The Netherlands, 9–13 August 2010; pp. 625–636.
44. Barandas, M.; Folgado, D.; Fernandes, L.; Santos, S.; Abreu, M.; Bota, P.; Liu, H.; Schultz, T.; Gamboa, H. TSFEL: Time Series Feature Extraction Library. *SoftwareX* **2020**, *11*, 100456. [CrossRef]
45. Santos, A.; Rodrigues, J.; Folgado, D.; Santos, S.; Fujao, C.; Gamboa, H. Self-Similarity Matrix of Morphological Features for Motion Data Analysis in Manufacturing Scenarios. In Proceedings of the 14th International Joint Conference on Biomedical Engineering Systems and Technologies (BIOSTEC 2021)—Volume 4: BIOSIGNALS, Virtual Event, 11–13 February 2021; pp. 80–90.
46. Chawla, N.; Bowyer, K.; Hall, L.; Kegelmeyer, W. SMOTE: Synthetic Minority Over-sampling Technique. *J. Artif. Intell. Res. (JAIR)* **2002**, *16*, 321–357. [CrossRef]

47. Wilson, D.J. The harmonic mean p-value for combining dependent tests. *Proc. Natl. Acad. Sci. USA* **2019**, *116*, 1195–1200. [CrossRef] [PubMed]
48. Yeo, I.K.; Johnson, R.A. A New Family of Power Transformations to Improve Normality or Symmetry. *Biometrika* **2000**, *87*, 954–959. [CrossRef]
49. Vallat, R. Pingouin: Statistics in Python. *J. Open Source Softw.* **2018**, *3*, 1026. [CrossRef]
50. JASP Team. JASP (Version 0.18.0) [Computer Software] . 2023. Available online: https://jasp-stats.org/ (accessed on 31 July 2023).
51. Guyton, A.C.; Hall, J.E. O Coração. In *Tratado de Fisiologia Médica*, 11th ed.; Elsevier: Amsterdam, The Netherlands, 2006; pp. 123–130.
52. Li, H.; Boulanger, P. A Survey of Heart Anomaly Detection Using Ambulatory Electrocardiogram (ECG). *Sensors* **2020**, *20*, 1461. [CrossRef]
53. Garber, C.; Blissmer, B.; Deschenes, M.; Franklin, B.; Lamonte, M.; Lee, I.M.; Nieman, D.; Swain, D. Quantity and Quality of Exercise for Developing and Maintaining Cardiorespiratory, Musculoskeletal, and Neuromotor Fitness in Apparently Healthy Adults: Guidance for Prescribing Exercise. *Med. Sci. Sport. Exerc.* **2011**, *43*, 1334–1359. [CrossRef] [PubMed]
54. Guyton, A.; Hall, J.E., The Autonomic Nervous System and the Adrenal Medulla. In *Textbook of Medical Physiology*, 11th ed.; Elsevier: Amsterdam, The Netherlands, 2006.
55. Sammito, S.; Thielmann, B.; Seibt, R.; Klussmann, A.; Weippert, M.; Böckelmann, I. Guideline for the application of heart rate and heart rate variability in occupational medicine and occupational science. *ASU Int.* **2015**, *2015*, 1–29. [CrossRef]
56. Brockmann, L.; Hunt, K.J. Heart Rate Variability Changes with Respect to Time and Exercise Intensity during Heart-rate-controlled Steady-state Treadmill Running. *Sci. Rep.* **2023**, *13*, 8515. [CrossRef] [PubMed]
57. Bigger, J.T.; Fleiss, J.L.; Steinman, R.C.; Rolnitzky, L.M.; Schneider, W.J.; Stein, P.K. RR Variability in Healthy, Middle-Aged Persons Compared with Patients with Chronic Coronary Heart Disease or Recent Acute Myocardial Infarction. *Circulation* **1995**, *91*, 1936–1943. [CrossRef] [PubMed]
58. Dekker, J.M.; Schouten, E.G.; Klootwijk, P.; Pool, J.; Swenne, C.A.; Kromhout, D. Heart Rate Variability from Short Electrocardiographic Recordings Predicts Mortality from All Causes in Middle-aged and Elderly Men: The Zutphen Study. *Am. J. Epidemiol.* **1997**, *145*, 899–908. [CrossRef] [PubMed]
59. Mang, Z.A.; Realzola, R.A.; Ducharme, J.; Bellissimo, G.F.; Beam, J.R.; Mermier, C.; de Castro Magalhaes, F.; Kravitz, L.; Amorim, F.T. The Effect of Repetition Tempo on Cardiovascular and Metabolic Stress When Time Under Tension is Matched During Lower Body Exercise. *Eur. J. Appl. Physiol.* **2022**, *122*, 1485–1495. [CrossRef] [PubMed]
60. Åstrand, I. Circulatory Responses to Arm Exercise in Different Work Positions. *Scand. J. Clin. Lab. Investig.* **1971**, *27*, 293–297. [CrossRef] [PubMed]
61. Tsuji, H.; Venditti, F.J.; Manders, E.S.; Evans, J.C.; Larson, M.G.; Feldman, C.L.; Levy, D. Determinants of heart rate variability. *J. Am. Coll. Cardiol.* **1996**, *28*, 1539–1546. [CrossRef] [PubMed]
62. Braun, S. Respiratory Rate and Pattern. In *Clinical Methods: The History, Physical, and Laboratory Examinations*, 3rd ed.; Walker, H., Hall, W., Hurst, J., Eds.; Butterworths: Boston, MA, USA, 1990; Chapter 43. Available online: https://www.ncbi.nlm.nih.gov/books/NBK365/ (accessed on June 2023).
63. Benditt, J.; McCool, F. The Respiratory System and Neuromuscular Diseases. In *Murray and Nadel's Textbook of Respiratory Medicine*; Elsevier: Amsterdam, The Netherlands, 2016; pp. 1691–1706.e4. [CrossRef]
64. Yuan, G.; Drost, N.A.; McIvor, R.A. Respiratory rate and breathing pattern. *McMaster Univ. Med. J.* **2013**, *10*, 23–25.
65. Cohen, C.A.; Zagelbaum, G.; Gross, D.; Roussos, C.; Macklem, P.T. Clinical manifestations of inspiratory muscle fatigue. *Am. J. Med.* **1982**, *73*, 308–316. [CrossRef]
66. Strang, A.; Ryan, L.; Rahman, T.; Balasubramanian, S.; Hossain, J.; Heinle, R.; Shaffer, T.H. Measures of respiratory inductance plethysmography (RIP) in children with neuromuscular disease. *Pediatr. Pulmonol.* **2018**, *53*, 1260–1268. [CrossRef] [PubMed]
67. Couser Jr, J.I.; Martinez, F.J.; Celli, B.R. Respiratory Response and Ventilatory Muscle Recruitment During Arm Elevation in Normal Subjects. *Chest* **1992**, *101*, 336–340. [CrossRef] [PubMed]
68. Hudson, A.L.; Butler, J.E.; Gandevia, S.C.; De Troyer, A. Interplay between the Inspiratory and Postural Functions of the Human Parasternal Intercostal Muscles. *J. Neurophysiol.* **2010**, *103*, 1622–1629. [CrossRef] [PubMed]
69. Celli, B.R.; Criner, G.; Rassulo, J. Ventilatory Muscle Recruitment During Unsupported Arm Exercise in Normal Subjects. *J. Appl. Physiol.* **1988**, *64*, 1936–1941. [CrossRef] [PubMed]
70. Hodges, P.; Gandevia, S. Activation of the human diaphragm during a repetitive postural task. *J. Physiol.* **2000**, *522 Pt 1*, 165–75. [CrossRef] [PubMed]
71. Sadat-Mohammadi, M.; Shakerian, S.; Liu, Y.; Asadi, S.; Jebelli, H. Non-invasive physical demand assessment using wearable respiration sensor and random forest classifier. *J. Build. Eng.* **2021**, *44*, 103–279. [CrossRef]
72. Tsai, M.K. Applying Physiological Status Monitoring in Improving Construction Safety Management. *KSCE J. Civ. Eng.* **2017**, *21*, 2061–2066. [CrossRef]

Disclaimer/Publisher's Note: The statements, opinions and data contained in all publications are solely those of the individual author(s) and contributor(s) and not of MDPI and/or the editor(s). MDPI and/or the editor(s) disclaim responsibility for any injury to people or property resulting from any ideas, methods, instructions or products referred to in the content.